Original Article

Investigating the Impact of Voxel Size and Postfiltering on Quantitative Analysis of Positron Emission Tomography/Computed Tomography: A Phantom Study

Ahmed Abdel Mohymen, Hamed Ibrahim Farag, Sameh M. Reda[1], Ahmed Soltan Monem[2], Said A. Ali[2]

Department of Nuclear Medicine and Radiation Therapy, National Cancer Institute, Cairo University, [1]Department of Radiometry, National Institute of Standards, [2]Department of Biophysics, Faculty of Science, Cairo University, Giza, Egypt

Abstract

Aim: This study aims to investigate the influence of voxel size and postfiltering on the quantification of standardized uptake value (SUV) in positron emission tomography/computed tomography (PET/CT) images. **Materials and Methods:** National Electrical Manufacturers Association phantom with the spheres of different sizes were utilized to simulate the lesions. The phantom was scanned using a PET/CT scanner, and the acquired images were reconstructed using two different matrix sizes, (192 × 192) and (256 × 256), and a wide range of postfiltering values. **Results:** The findings demonstrated that postfiltering significantly affected SUV measurements. The changes in postfiltering values can result in overestimation or underestimation of SUV values, highlighting the importance of carefully selecting appropriate filters. Increasing the matrix size improved SUVmax and SUVmean values, particularly for small-sized spheres. Smaller voxel reconstructions slightly reduced partial volume effects and partially enhanced SUV quantification. **Conclusions:** Careful consideration of postfiltering values and matrix size selection can lead to better SUV quantification. These findings emphasize the need to optimize the reconstruction parameters to enhance the clinical utility of PET/CT in detecting and evaluating malignant lesions.

Keywords: Gibbs artefact, partial volume effects, point spread function, postfiltering, time of flight, voxel size

Received on: 21-07-2024 **Review completed on: 17-08-2024** **Accepted on: 22-08-2024** **Published on: 18-12-2024**

Introduction

Positron emission tomography/computed tomography (PET/CT) is a highly valuable tool in the early detection of lesions due to its excellent sensitivity and specificity.[1] However, when utilizing PET/CT to quantify the activity concentration (kBq/ml) of lesions, there are several ill-posed factors, both biological and technological factors, can impede accurate standardized uptake value (SUV) measurements.[2-4] Among the technological factors that significantly affect the SUV quantification of PET/CT images is the degradation of spatial resolution.[5,6]

Partial volume effects (PVEs) arise from two primary sources: the limited spatial resolution of the PET system and the finite voxel size in the reconstructed image. PVE can lead to tissue-fraction effects (TFEs), where a voxel may contain a combination of multiple tissues classes due to limited spatial resolution. The limited spatial resolution leads to blurred lesion boundaries.[7-9] PVE can significantly influence both the qualitative and quantitative analysis of PET/CT images. This effect becomes particularly pronounced when the size of a lesion is less than three times the full width at half maximum (FWHM) of the reconstructed image resolution.[7,10] Moreover, PVE affects the apparent size and shape of the lesion, which can be problematic when using PET for radiotherapy treatment planning.[10,11]

Although lesion size, shape, and uptake in surrounding tissues cannot be controlled, the impact of PVE depends on the parameters that can be tuned. One crucial parameter is the spatial resolution in the reconstructed images. Higher

Access this article online

Quick Response Code:

Website: www.jmp.org.in

DOI: 10.4103/jmp.jmp_123_24

Address for correspondence: Dr. Said A. Ali, Department of Biophysics, Faculty of Science, Cairo University, Giza, Egypt. E-mail: saidataha@cu.edu.eg

How to cite this article: Mohymen AA, Farag HI, Reda SM, Monem AS, Ali SA. Investigating the impact of voxel size and postfiltering on quantitative analysis of positron emission tomography/computed tomography: A phantom study. J Med Phys 2024;49:597-607.

spatial resolution minimizes the spread of lesion, while lower spatial resolution introduces a significant amount of spread. Consequently, a given lesion will exhibit variations in size, brightness, and SUV depending on the spatial resolution.[11,12]

Reconstruction parameters, (such as number of iterations, subsets, postfiltering, and voxel size), are considered the significant factors that influence the spatial resolution of PET/CT images.[13] Therefore, the choice of these parameters can partially control PVE, as better spatial resolution results in less pronounced PVE.[14,15] Since PVE is partly caused by finite spatial resolution, iterative deconvolution approaches have been proposed to estimate the spillover effect generated by the point spread function (PSF) of PET scanner.[16,17] Applying PSF modeling as a postreconstruction deconvolution technique improves the spatial resolution and SNR of iterative algorithms. However, it can also cause higher-resolution, edge-overshoot, and degraded spatial resolution.[18,19] Applying postfiltering during the reconstruction process regarded as one of the main factors influencing the degree of edge artifacts.[20,21] In addition to PSF algorithm, the incorporation of Time-of-Flight (TOF) information into PET images reconstruction process provided images with higher signal-to-noise ratios (SNRs).[22] Combining TOF and PSF allows for leveraging the advantages of both of them. Therefore, while TOF acts as an "accelerator" for signal convergence, PSF can yield a better signal with fewer iterations, simultaneously introducing a "filtering" effect that reduces noise in the reconstructed TOF-PSF images.[23,24]

The current work aims to assess the effects of voxel size and postfiltering (mm) on SUV quantification for various sphere sizes utilizing a TOF-PSF-based reconstruction algorithm in PET/CT imaging.

Materials and Methods

In this work, the authors utilized the National Electrical Manufacturers Association (NEMA) and International Electro technical Commission body phantom and imaging protocol.[25,26]

Phantoms

Cylindrical phantom (flood phantom)

As the part of the current study, a cross-calibration factor was investigated to assess the synchronization of activity concentrations (kBq/ml) between the estimated activity concentrations values obtained from PET images using a PET scanner and the expected activity concentration values measured by a dose calibrator. A solution of ^{18}fludeoxyglucose (FDG) (37 MBq, as measured by the dose calibrator) was introduced into a cylindrical phantom with interior dimensions of 8.5" diameter × 7.32" height (21.6 cm × 18.6 cm) and a precisely known volume of 6.9 L. Subsequently, the phantom was filled with water to achieve a solution with a precisely known activity concentration. A single-bed acquisition of the phantom was performed and the raw data of PET-phantom images were reconstructed with attenuation and scatter correction settings identical to those used for patient studies.

Upon the completion of the images reconstruction, the SUVmean (kBq/ml) was measured by defining a region of interest (ROI) with a diameter that was at least 3 cm smaller than the diameter of the uniform cylindrical phantom, on one transverse slice and then copying that ROI, to all consecutive transverse slices (except the first and the last slice). The average of mean SUVs for all ROIs throughout the phantom was calculated as measured by the PET scanner. To calculate the cross-calibration factor, the average activity concentration of the phantom PET images measured using the PET scanner was divided by the activity concentration measured using the dose calibrator at the beginning of filling the phantom, the manufacturer recommended that "The ROI readout should equal the kBq/ml ± 10%."[27] In the present work, the cross-calibration factor was found to be 0.91, which is aligned with the recommended value provided by.[4,27] In addition, the clocks of the PET acquisition workstation and the dose calibrator were synchronized.

National Electrical Manufacturers Association body phantom

The NEMA body phantom's specifications included: an interior length of 18 cm, a background compartment with a volume of 9.7 L, a precisely known volume of 9.7 L, cylindrical insert dimensions of an outside diameter of 51 mm and a length of 180 mm. It was equipped with six fillable spheres of varying inner size diameters: 10, 13, 17, 22, 28, and 37 mm.

At the start of the measurements, the background compartment and spherical inserts were filled with ^{18}FDG solutions containing 2.0 and 20 kBq/mL, respectively. As a result, the sphere-to-background ratio was 10 to 1. The current study utilized phantom imaging procedures by positioning the phantom at the PET/CT table and aligning it using the CT laser marker in accordance with the NEMA NU 2-2007 guidelines. For phantom scanning, two bed position was performed and the scanning duration was set to be 5 min for each bed position.[28,29]

Data acquisition

For the imaging procedures, a PET/CT Discovery 710 installed at National Cancer Institute – Cairo university by GE Healthcare (Milwaukee, WI, USA) was used, in accordance with the current EANM/EARL guidelines for ^{18}FDG Image Quality QC phantom imaging.[25,30] The data acquisition and images reconstruction were performed using the software implemented in the Discovery 710 PET/CT Advantage Workstation Volume Share 5 (AW 4.6) release. The technical specifications of the PET/CT Discovery 710 system are found in Table 1.[31]

Image reconstruction

The current study focused on evaluating the impact of the matrix size and postfiltering on SUV measurements. The PET/CT phantom images were reconstructed with 2 iterations and 18 subsets for two different matrices sizes: 192 × 192 and 256 × 256, resulting in pixels sizes of 3.64 and 2.73 mm, respectively. Postreconstruction filters with FWHM ranging from 4 to 10 mm, in increments of 0.5 mm, were also applied. A fully three-dimensional maximum-likelihood ordered subset expectation maximization algorithm combining with

Table 1: Technical characteristics of discovery 710 positron emission tomography/computed tomography scanner[31]

PET detector	Specifications
Gantry dimensions (cm)	192×226.1×140
Weight (kg)	4916
Patient port (cm)	70
Scintillator material	LYSO
Scintillator dimensions (mm)	4.2×6.3×25
Crystal array per block	9×6
Number of detector rings	24
Number of crystals per ring	576
Number of crystals	13,824
Number of PMTs	1024 (256 quad-anode)
Number of image planes	47
Vertical travel (cm)	2.5–20.5 below the isocenter
Acquisition modes	3D, 4D
Coincidence window (ns)	4.9
Lower energy threshold (keV)	425
Maximum axial coverage (cm)	170–200
Axial field of view (cm)	15.7
Transaxial field of view (cm)	70
Slice overlap	User defined 1–23, minimum recommendation 5 (10% overlap)
Image matrix sizes	128×128, 192×192, 256×256
Transmission source	CT attenuation correction

3D: Three-dimensional, 4D: Four-dimensional, PET: Positron emission tomography, CT: Computed tomography, PMTs: Photo-multiplier tubes

TOF + PSF, ("Vue Point FX + Sharp IR"), were used for PET/CT-NEMA phantom images reconstruction with all corrections applied. The reconstructed images had a slice thickness of 3.25 mm. The Sharp IR method is an advanced system modeling technique that enhances visual contrast and resolution in whole-body PET images.[31]

Data analysis

In this study, the analysis of PET/CT reconstructed images was conducted using a GE Healthcare Advantage Workstation. The software's processing tools were employed to delineate the percentage of volume of interest at 50% (VOI50%) on PET images for each sphere, utilizing the predefined XY plane. To ensure consistency, the reconstructed PET slice containing the largest diameter among all spheres was selected to adjust the VOI50% measurements. Following the image quality assessment guidelines outlined by NEMA NU 2-2007, the SUVmax (maximum SUV) and SUVmean (mean SUV) were determined for all spherical inserts. The SUVs values for the six spherical inserts were calculated based on the 50% background-corrected isocontour VOI (SUVmean) and the maximum voxel value included in the VOI (SUVmax). For the $SUV_{\text{background}}$, for each sphere, a six ROIs of fixed dimensions (diameters equal to the physical inner diameter of the spheres) were defined. They were placed in regions that did not contain any hot sphere, and they were not allowed to intersect. Taking the mean SUV of 6 ROIs for each sphere resulted in the $SUV_{\text{background}}$ used for RC calculation. SUVmean incorporates information from multiple voxels, making it less sensitive to image noise. However, it is subject to intraobserver and interobserver variability. On the other hand, SUVmax represents the highest voxel value within the VOI and is independent of VOI definition, but it is more susceptible to noise.[3]

Quantitative analysis

The recovery coefficient (RC) was employed as a quantitation method to assess the effect of matrices sizes and postfilterings on SUVs measurements of hot spherical inserts in reconstructed images. A background correction factor was applied to all RCs values. The RC was defined as follows:

$$\text{RC} = \frac{\text{SUVMeasured in sphere-Measured SUVbackground}}{\text{SUVCalculated in sphere-Calculated SUVbackground}}$$

where,

[SUV_{Measured}, estimated (max and mean) activity concentration in (kBq/ml) measured from the reconstructed PET images of phantom].

[$SUV_{\text{Calculated}}$, expected activity concentration in (kBq/ml) measured by dose calibrator during filling of spherical inserts].[32]

$SUV_{\text{background,}}$ mean activity concentration in (kBq/ml) measured from the reconstructed PET images of background compartment of NEMA phantom.

The RC served as a valuable metric to assess the concordance between the measured and calculated SUVs values, with the ultimate goal of achieving a RC of unity. This means that when RC equals unity, it suggests a perfect recovery where the measured SUV matches the calculated SUV.

Results

The effects of different postfiltering values and matrices sizes on the SUVs quantification were investigated as follows:

Impact of Gaussian postfiltering on the standardized uptake values quantification

The first part of the current study focused on Gaussian postfiltering with increments of 0.5 mm and ranges from 4 to 10 mm. The current study's observations were made at 2 iterations and 18 subsets for two different matrices sizes: 192 × 192 and 256 × 256. These observations are depicted in [Figures 1-4]. The RC was utilized as the metric with the ideal outcome being a value of unity. However, deviations from this ideal behavior may occur and result in either overestimation or underestimation of RCs values due to inappropriate postfiltering selection. When a 4-mm postfilter was applied, it resulted in the overestimation of RCs values for all spheres sizes except at 10 mm sphere. There was a slight overestimation in RCmean of the 37 and 17 mm spheres at postfilters of 4, 4.5, and 5 mm and a 192 × 192 matrix size. In terms of RCmax, the 17 mm sphere showed a significant overestimation/overshooting compared to the 22 and 13 mm spheres at both matrices sizes. In addition, when a 4-mm postfilter

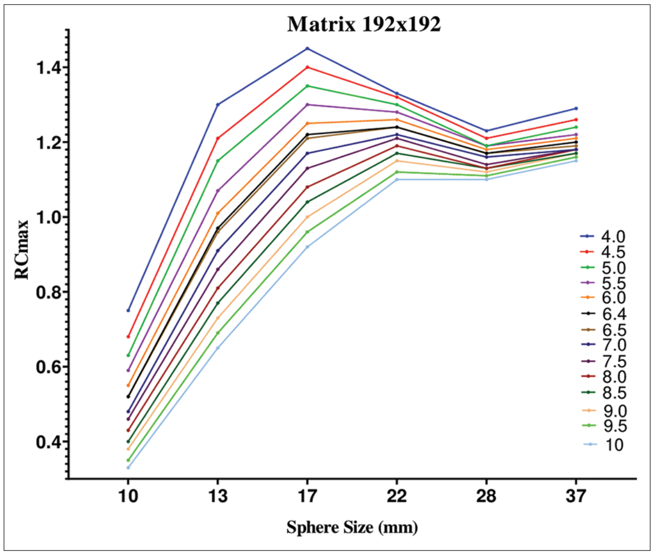

Figure 1: The relation between RCmax and sphere sizes (mm) at matrix 192 × 192 for a wide range of postfiltering values

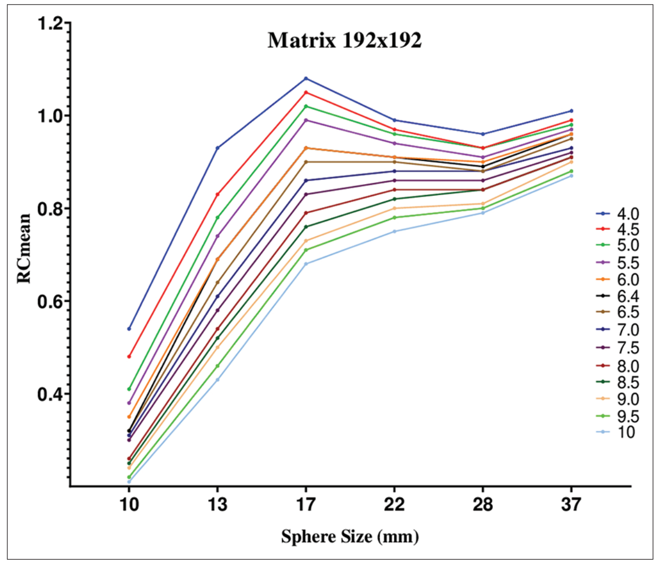

Figure 2: The relation between RCmean and sphere sizes (mm) at matrix 192 × 192 for a wide range of postfiltering values

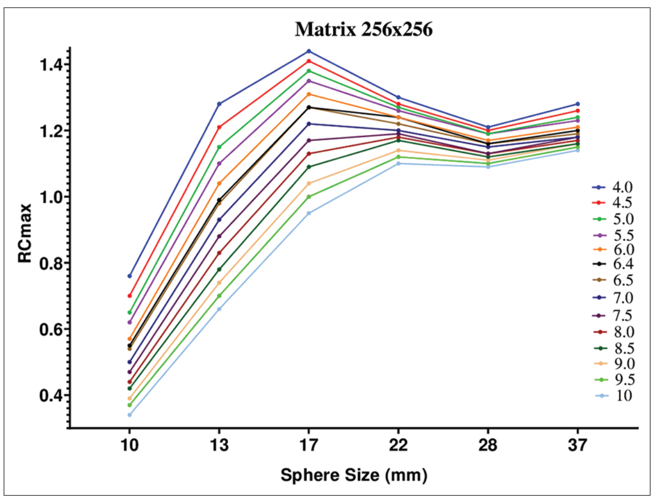

Figure 3: The relation between RCmax and sphere sizes (mm) at matrix 256 × 256 for a wide range of postfiltering values

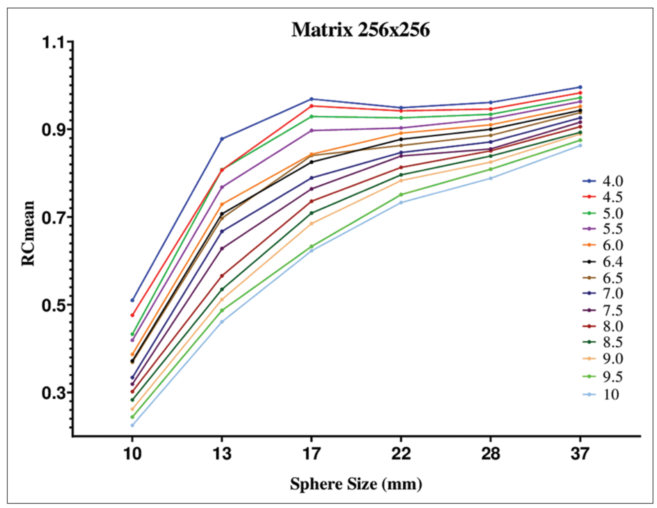

Figure 4: The relation between RCmean and sphere sizes (mm) at matrix 256 × 256 for a wide range of postfiltering values

was applied at 10 mm sphere, it resulted in underestimation in RCmax and RCmean values, RCmean exhibited a more pronounced underestimation. As the postfiltering values increase, the underestimation effect became more prominent. At 256 × 256 matrix size, there was no overshooting observed in RCmax and RCmean values when postfilters of 10 and 5.5 mm were applied, respectively. The current study highlighted that RCmean was less affected by overestimation and overshooting compared to RCmax. At 192 × 192 matrix size, the overshooting effect in RCmax of 17 and 13 mm spheres ceased at 7.5 mm and 4.5 postfilterings, respectively. However, the overestimation in RCmax of 22 mm sphere persisted until the postfiltering value reached 10 mm. In addition, there was no overshooting observed for any spheres sizes at postfilters 10 and 7 mm for RCmax and RCmean, respectively. The increasing in postfiltering values slightly mitigated the overestimation and overshooting in RCmax at large spheres and unfortunately resulted in significant increase in the underestimation of RCmax at small spheres. This trade-off sacrificed the detectability of small spheres, as illustrated in Figures 5 and 6.

Figures 7-10 depict the effects of different postfiltering values on the ideal scenario of RCs. In Figure 7, at a postfiltering level of 10 mm, RCmax exhibited a consistent decrease as sphere sizes decreased, ultimately eliminating overshooting. Similarly, Figure 8 demonstrates a monotonic decrease in RCmean at a postfiltering level of 7 mm, leading to the cessation of overestimation and overshooting. Figure 9 shows the impact of the lowest and highest postfiltering values on the RCmax of spheres with different sizes in a 256 × 256 matrix. Finally, Figure 10 depicts a monotonic decrease in RCmean at a postfiltering 5.5 mm with decreasing sphere sizes, resulting in the elimination of overestimation and overshooting.

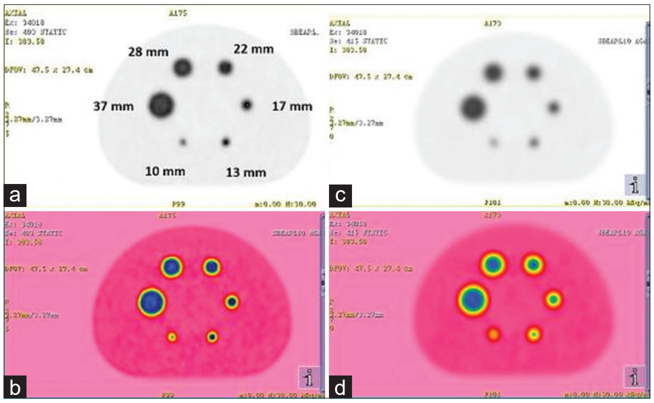

Figure 5: The reconstructed National Electrical Manufacturers Association phantom images. This figure shows the impact of postfiltering value on standardized uptake value quantification. It is divided into (a and b) and (c and d), for 4 and 10 mm postfilters, respectively. 2 iteration, 18 subset and 192 × 192 matrix size were used

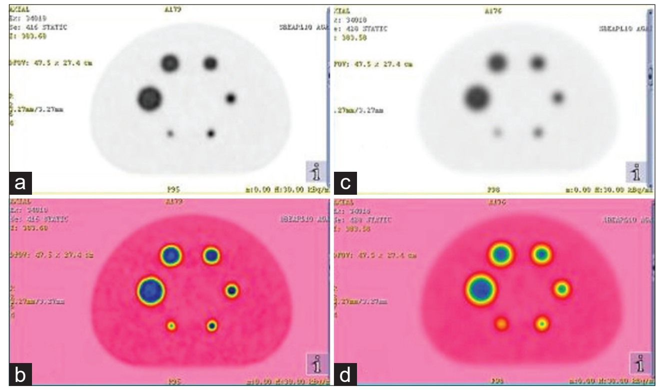

Figure 6: The reconstructed National Electrical Manufacturers Association phantom images. This figure shows the impact of postfiltering value on standardized uptake value quantification. It is divided into (a and b) and (c and d) for 4 and 10 mm postfilters, respectively. 2 iteration, 18 subset and 256 × 256 matrix size were used

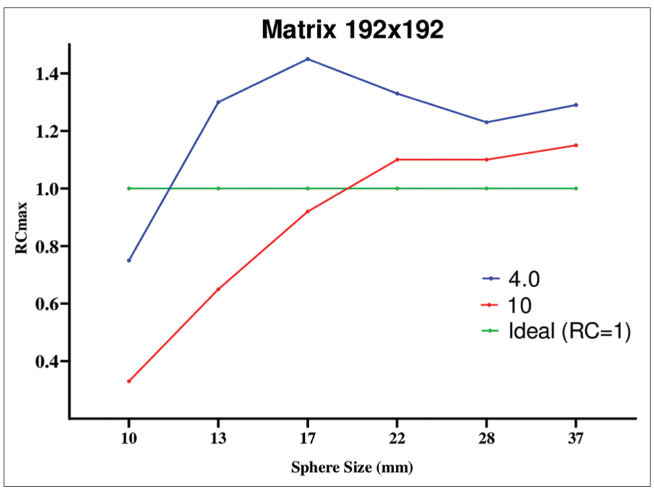

Figure 7: The impact of lowest and highest postfiltering on RCmax of different sphere sizes (mm) at matrix 192 × 192. At postfiltering 10 mm, RCmax decreased monotonically with decreasing sphere sizes and the overshooting was ceased and disappeared

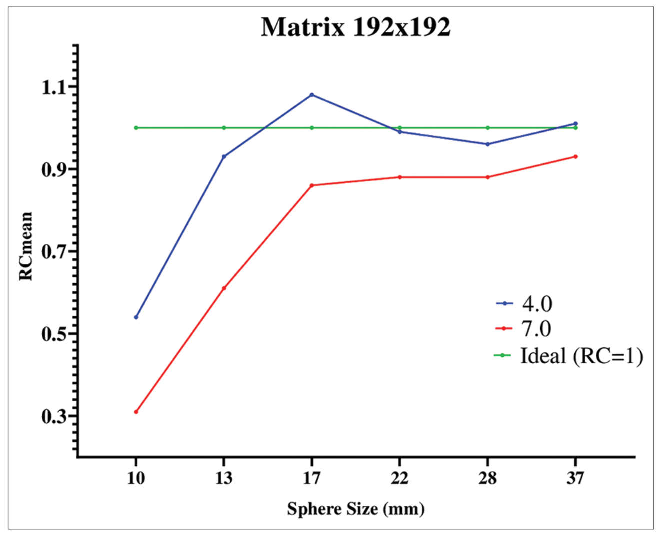

Figure 8: The impact of two different postfilterings on RCmean of different sphere sizes (mm) at matrix 192 × 192. At postfiltering 7 mm, RCmean decreased monotonically with decreasing sphere sizes and the overestimation and overshooting were ceased and disappeared

In ideal situation, RCs should be unity, indicating a precise SUVs quantification. However, the overestimation in SUVs occurred when RCs values exceeded unity, while the underestimation occurred when RCs fell below unity. Overshooting in RCs values indicated a nonmonotonic behavior, where RCs values decreased inconsistently with decreasing spheres sizes. These instances of overestimation and overshooting in RCs values reflect the fluctuations in SUVs, which eventually affects SUV quantification.

When the two matrices sizes were compared, within the range of postfilterings from 4 to 5 mm, RCmean demonstrated superior performance over RCmax in quantifying SUVs for larger spheres measuring 17 mm or more. This advantage of RCmean can be attributed to its ability to minimize the impact of overestimation and overshooting caused by Gibbs artifact, as illustrated in [Figures 11a, b and 12a, b]. Conversely, for the postfilterings ranging from 5.5 to 6.5 mm, RCmax outperformed RCmean in quantifying SUVs for smaller spheres measuring 13 mm or less. However, it is important to note that outperformance achieved by RCmax was significantly influenced by overestimation and overshooting caused by Gibbs artifact.

Influence of postfiltering on standardized uptake values quantification: Insights from Gibbs artifact visualization at (192 × 192) and (256 × 256) matrices

The visualization of Gibbs artifacts at 192 × 192 and 256 × 256 matrices sizes, Figures 5 and 6, respectively, revealed distinct patterns when examining large and small spheres. As shown in [Figures 5b, d and 6b, d], the blue color, representing density, displayed intriguing characteristics depending on the size of the sphere. When a 4-mm postfiltering value was applied, the impact on the visualization became evident. The blue color corresponded to the RC. Interestingly, the presence of overestimations and overshootings in the RCs was observed. This

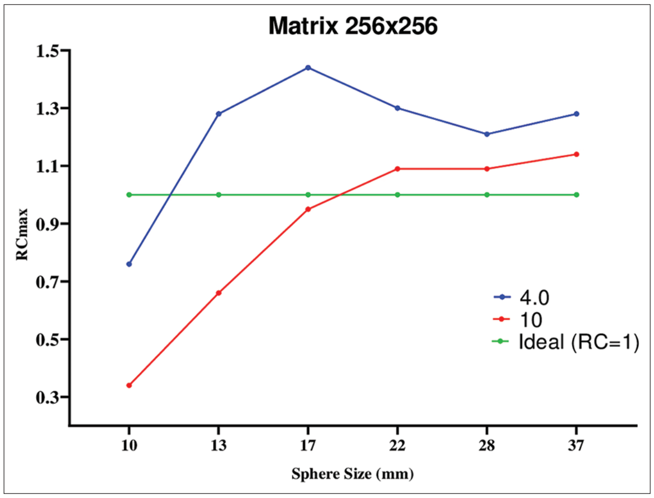

Figure 9: The impact of lowest and highest postfiltering on RCmax of different sphere sizes (mm) at matrix 256 × 256. At postfiltering 10 mm, RCmax decreased monotonically with decreasing sphere and the overshooting was ceased and disappeared

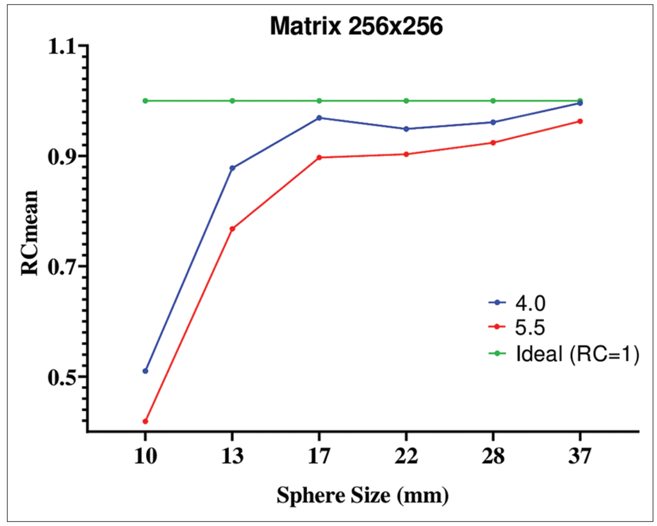

Figure 10: The impact of two different postfilterings on RCmean of different sphere sizes (mm) at matrix 256 × 256. At postfiltering 5.5 mm, RCmean decreased monotonically with decreasing sphere sizes and the overestimation and overshooting were ceased and disappeared

observation indicated that the postfiltering process influenced the presence of Gibbs artifacts and led to an increasing or decreasing in their magnitude. The analysis of [Figures 5 and 6] demonstrated that, for both matrices sizes, the dense blue color was primarily concentrated at the periphery of the large sphere. This concentration was attributed to the presence of Gibbs artifacts and suggested that the postfiltering process had a stronger impact on the outer regions of the large spheres. Conversely, for the small sphere, the dense blue color was concentrated at the center which was also due to the influence of Gibbs artifacts. This indicated that the postfiltering process had a more pronounced effect on the central region of the small sphere and resulted in significant modifications to its appearance, as illustrated in [Figures 5a, b and 6a, b]. Furthermore, as the postfiltering values increased, the dense blue color associated with Gibbs artifacts gradually decreased, as depicted in [Figures 5c, d and 6c, d]. This monotonic decrease in the intensity of the blue color was specifically observed at the postfiltering value 10 mm and 192 × 192 matrix. A similar trend was noticed at 256 × 256 matrix, although with slight variations in the density of the blue color at the periphery and center of the large and small spheres, respectively. These variations suggested that the postfiltering process had a more pronounced effect on certain regions "(peripheral or central regions according to sizes of imaged spheres)" and resulted in a uniform distribution of the blue color intensity, as demonstrated in [Figures 5d and 6d]. [Figure 5a and b] which highlighted the presence of Gibbs artifacts as overshoots along the edges of the spheres having a diameter of 17 mm or larger. However, in spheres having a diameter of 13 mm or smaller, the artifacts appeared in the center. These artifacts led to an overestimation of the RC for larger spheres. Conversely, small spheres typically experienced an underestimation of its RCs due to PVE. Interestingly, the presence of Gibbs artifacts in small size spheres causing a partial compensation for the underestimation in RCs values occurred due to PVE and thereby improving the overall RCs values. These observations were consistent with what was found by other investigators.[18,26] In summary, the visualization of the impact of the postfiltering values at both matrices revealed significant findings. The overestimation and overshooting in the RC were clearly observed at 4-mm postfiltering and accompanied by a nonuniform distribution in color density within the spheres. The dense blue color indicated different regions of concentration depending on the size of the sphere, postfiltering values, and matrices sizes. At 10-mm postfiltering, the dense blue color associated with Gibbs artifacts gradually decreased for both the large and small spheres and resulted in a uniform distribution of the blue color density inside the spheres. The visualization of Gibbs artifacts at different postfiltering values and matrices sizes showcased intriguing variations in the density of the blue color at the large and small spheres. The distribution of this color, whether denser at the periphery of larger spheres or at the center of smaller spheres, played a significant role in shaping the visual impact and the overall perception of Gibbs artifacts within the spheres.

Impact of matrix size on standardized uptake value quantification

In the second part of the present study, two different matrices sizes were compared to investigate their effects on SUVs quantification at various spheres sizes, as depicted in Figure 13. The results revealed that utilizing a larger matrix size of 256 × 256 slightly reduced the overestimation observed in RCmax values for the large spheres and partially compensated for the underestimation found at the small spheres, as shown in Figure 13. When analyzing spheres sizes larger than 10 mm at 4 mm postfiltering and 192 × 192 matrix size, a significant overestimation and overshooting in RCmax values was observed. However, this increase in RCmax was slightly mitigated when using a larger matrix size of 256 × 256, as illustrated in Figures 7-10. Furthermore, it was observed that the impact of a larger matrix size (256 × 256) on the RCs values was comparable to that of a wider postfiltering (in mm) and resulted in decreasing the

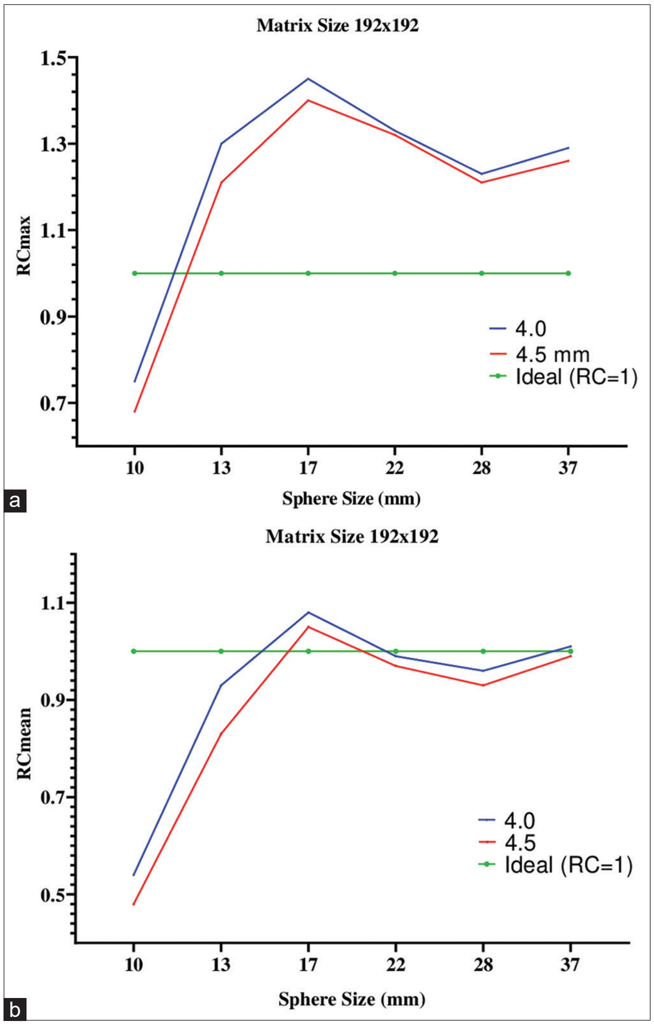

Figure 11: The impact of both 4 and 4.5 mm postfiltering on (a). For RCmax and (b). For RCmean for different sphere sizes (mm) at matrix 256 × 256

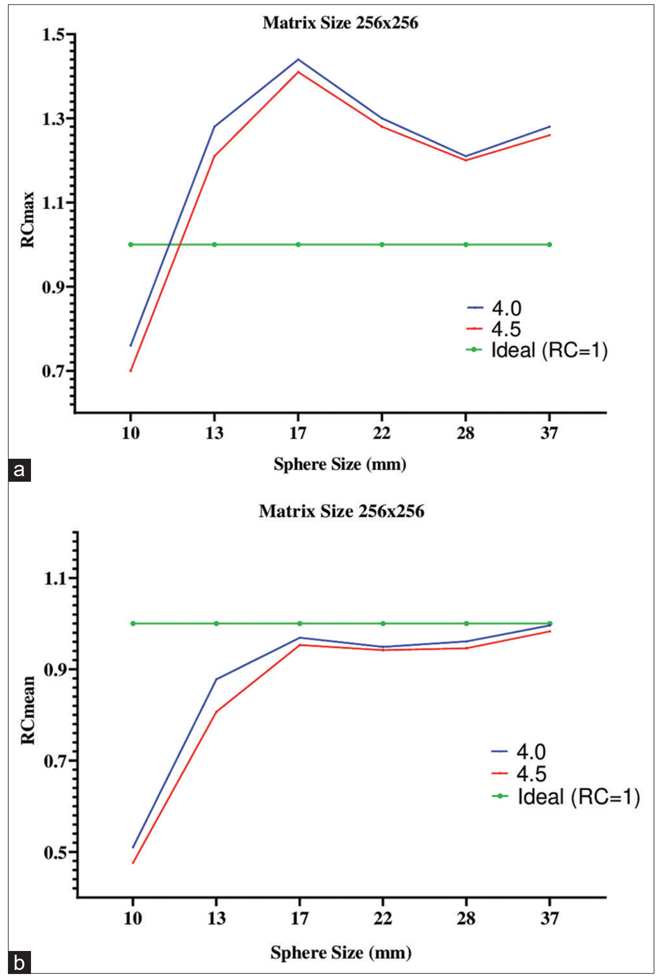

Figure 12: The impact of both 4 and 4.5 mm postfiltering on (a). For RCmax and (b). For RCmean for different sphere sizes (mm) at matrix 256 × 256

RCs values, as shown in Figures 5 and 6. Conversely, for larger spheres, the observed underestimation in RCmax of 10 mm sphere at a 4 mm postfiltering and 192 × 192 matrix size was partially compensated by the larger matrix size of 256 × 256. The RCmax value at 10 mm sphere increased from 0.33 to 0.34. This behavior was consistent across all postfiltering values at 10-mm sphere. For instance, at 6.4-mm postfiltering value, the RCmax values for spheres 22, 17, and 13 mm at a 192 × 192 matrix size were 1.24, 1.22, and 0.97, respectively. When using a 256 × 256 matrix size, the RCmax values became 1.24, 1.27, and 0.99, respectively. Hence, the larger matrix size had a minimal effect on RCs values for different spheres sizes. Furthermore, it was observed that 256 × 256 matrix size slightly improved the RCmax values as the postfiltering values increased, particularly for spheres sizes equal to or >13 mm. At 10-mm sphere size, it was preferable to use a small postfiltering value and a matrix size of 256 × 256. Overall, utilizing a 256 × 256 matrix size with an appropriate postfiltering value reduced the underestimation and overshooting observed in the RCs values compared to 192 × 192 matrix size.

Based on the obtained findings, the present study demonstrated that Gibbs artifact and PVE phenomenon had an impact on SUVs quantification. Gibbs artifact resulted in overestimation and overshooting of the RCs values (RCs values larger than unity) for large spheres sizes, while PVE caused underestimation of the RCs values (RCs values less than unity) for small spheres sizes. These over/underestimations of the RCs values at different spheres sizes accounted for the fluctuations observed during SUVs quantification. Since SUVmax is more sensitive to noise than SUVmean, the SUVmax of large spheres was highly influenced by the negative impact of Gibbs artifact compared to SUVmean. Therefore, when dealing with spheres sizes larger than 13 mm, it is advisable to use SUVmean with a large matrix size and an appropriate postfiltering value. On the other hand, for small spheres sizes, SUVmax was preferred because the overestimation caused by Gibbs artifact had a positive impact and partially compensated for the underestimation in the RCs values due to PVE phenomena.

In conclusion, a larger matrix size had a less significant effect on SUVs quantification than the postfiltering effects. It is crucial to carefully select the appropriate matrix size and

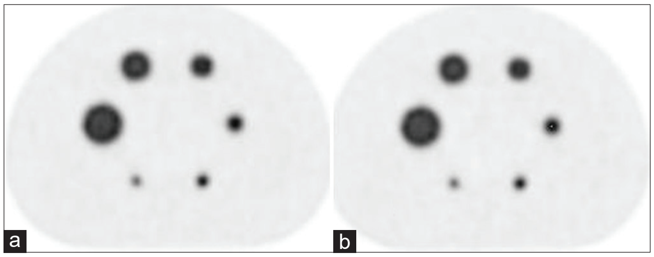

Figure 13: The reconstructed phantom images. This figure shows the impact of 192 × 192 (a) and 256 × 256 (b) matrix sizes on standardized uptake value quantification. Postfilter 4 mm, 2 iteration, and 18 subset were used

adequate postfiltering value to ensure accurate and reliable SUVs measurements in PET/CT imaging. These findings provide valuable insights into the impact of the postfiltering values and voxels sizes on SUVs quantification and can assist in optimizing the reconstruction parameters for improving accuracy and reliability in future PET/CT imaging studies.

Discussion

The purpose of the present study is to investigate how the changing in voxels sizes and postfiltering values effects on the SUVs quantification. The SUVs quantification was affected by two types of artifacts, noise artifact and Gibbs artifact. The noise artifact arises from unconstrained maximum-likelihood image estimation at low activity concentrations, while the Gibbs artifact was more evident in images at a high activity concentration, accounting for PSF of PET scanner.[33] PVE occurs due to low system spatial resolution and finite voxel size.[8] At a small matrix size (larger voxel size), PVE increases the impact of the TFE due to the finite voxel size.[15,34] Imaging spatial resolution plays a crucial role in lesion detection, especially for small lesions, and the spillover effect causes activity concentration to spill out from hot lesions to warm background and vice versa.[35]

The obtained results demonstrated that small voxel reconstruction resulted in decreasing the overestimation/overshooting in the RCs values, as most high-frequency artifacts disappeared, these findings are aligned with those of a previous study.[6] Other scientists[33,36] discussed noise and Gibbs artifacts in PET imaging resulting from PSF algorithm and explored the development of postfilters to minimize their impacts. However, the magnitude of the overshoot and the diameter of the observed overshoot depend on several factors including activity concentration, pixel size, number of iterations, and FWHM (mm) of Gaussian filter.[37,38] Although PSF-based reconstruction can nearly achieve the minimum pixel variance for a given spatial resolution, caution should be taken when incorporating the PSF into reconstruction algorithm without any or minimal postfiltering applied, as it can introduce a significant SUV bias.[39] SUVmax represents the highest voxel value within the VOI and is independent of VOI definition, but it is more susceptible to noise. In contrast, SUVmean incorporates information from multiple voxels, making it less sensitive to image noise, but it is more dependent on VOI definition and subject to intra- and interobserver variability.[40] The impacts of PSF algorithm and PVE on the SUVs measurements can vary depending on the size of sphere under evaluation.[41] For larger spheres, the PSF artifact tends to affect the outermost voxels more than the innermost ones, resulted in overestimation of SUVmax. Conversely, PVE has a relatively lower impact on larger spheres since they are more likely to be entirely contained within a single voxel and produce a more accurate SUVmax measurement. On the other hand, for smaller spheres, the effects of PVE are more pronounced, as they are more susceptible to PVE. This often leads to underestimation in SUVmax and SUVmean, which consistent with Luebe *et al*.[9] In addition, the impact of PSF artifact on SUVs measurements was more significant for smaller spheres since the blurring effect becomes a more dominant factor in the overall SUVs measurements. Hence, it is crucial to consider the potential impacts of PSF and PVE artifacts on SUVs measurements when interpreting PET imaging results, especially when assessing lesions of different sizes. To mitigate these artifacts, we should be aware of the impact of different reconstruction parameters such as postreconstruction filtering (mm), voxel sizes, PSF, and TOF technologies. These factors can help to improve the accuracy of the SUVs measurements and increase the reliability of PET imaging results.

In the current work, the overshooting (Gibbs artifact) was observed at 13, 17, and 22 mm spheres sizes and this leads to overestimating the SUVs which is consistent with what was observed by Tong *et al*.[42] Moreover, larger matrix sizes and TOF-PSF-based reconstructions have been found to slightly enhance the SUVmax and SUVmean values. However, the present work indicated that higher matrix sizes can be overestimate SUVmean, although this effect was less pronounced than that for SUVmax, which is consistent with the findings obtained in a previous study.[43] The combination of TOF and PSF reconstruction in PET imaging can be advantageous in utilizing the strengths of each technique. TOF can accelerate signal convergence and results in increasing variation in image voxel variance ratios, while PSF can enable better signal recovery at lower iterations and reduce noise in reconstructed images.[26,44]

The observed overshooting in spheres sizes 17 and 22 mm was attributed to the presence of Gibbs artifact, which was commonly observed in large-voxel reconstruction, this finding is aligned with those of other studies.[45] The obtained results demonstrated that smaller matrix sizes (large voxels) can lead to higher RCmax values due to the increase in image noise which was confirmed by another study.[43] To adjust the impact of this effect, a convenient postfiltering value can be applied. It was observed that small voxel reconstruction can partially eliminate Gibbs artifact which is consistent with what was found by other researchers.[6] The present study found that 2-mm voxel reconstruction improved spatial resolution, reduced PVE, and affected the SUV values. These results are consistent with those of Zimmermann *et al*.[46] Small voxel reconstruction led to increasing the SUVmean and SUVmax for the small spheres with diameters < 13 mm which is consistent with what was found by other researchers.[22] This, in turn, increases the probability of sampling the peak uptake of small sizes spheres. In addition, larger matrix sizes can reduce PVE which is confirmed by earlier publications.[14,47] According to the Nyquist, sampling theorem, the optimal pixel size in PET imaging is half the spatial resolution. Larger pixel sizes lead to undersampling, causing aliasing, while smaller pixel sizes result in useless oversampling. Therefore, the choice of a 256 × 256 matrix with a 2.7 mm pixel size can significantly impact SUVs quantification.[48] The present study revealed that when reducing the postfiltering values, this led to increasing Gibbs artifact and overestimating SUVmax which is confirmed by other investigators.[49] On the other hand, a larger matrix improved the spatial resolution, while a smaller matrix reduced it. However, voxel size is a compromise between suppressing signal noise (requiring larger voxel size) and capturing small imaging details (requiring smaller voxel size), as SNR typically decreases with increasing voxel size. Typically, the selection of matrix size should ensure that pixel size which is approximately one-third of the spatial resolution of PET scanner.[50] The current work found that PVE phenomenon was more pronounced in small spheres sizes, such as those in spheres with a diameter <13 mm, resulting in reducing the measured activity concentrations at 4-mm voxel size. However, switching to a 2-mm voxel size can help reduce this effect. Conversely, for large spheres sizes, such as those in a sphere with a diameter of 37 mm, were less affected by the PVE.

Bettinardi *et al*.[23] had shown that incorporating TOF with PSF reconstruction can improve the noise resulting from small voxel reconstruction in PET imaging. The obtained findings were consistent with these previous studies which had also suggested that a larger matrix size (smaller voxels) resulted in minimizing Gibbs artifact and PVE. The present study revealed that large matrix size led to increasing the SUVs values and decreasing the PVE, particularly in small spheres which is consistent with what was found in a previous publication.[51] Moreover, previous studies had shown that combining of TOF with small voxel reconstruction can help in minimizing the impact of PVEs on small structures.[52,53] The current study demonstrated that wider postfiltering values can suppress PSF artifacts and restore the expected relationship where the RC decreases monotonically as sphere size decreases. However, these postfiltering values should not be too wide, as this can unnecessarily decrease the RCs, particularly in small spheres with a diameter <13 mm. what was found in a previous publications.[49,54]

The authors of the present study recommend using a small voxel reconstruction with appropriate postfiltering value, although a 4-mm pixel size is commonly used in PET oncology studies to reduce noise levels, it comes at the expense of poorer spatial resolution and contrast.[55] Unfortunately, the combined PSF and TOF algorithms may not have a significant effect on total noise levels in PET imaging, but they do cause a slight qualitative shift in the relative noise distributions. Therefore, it is important to be aware of these effects when analyzing PET imaging results.[24] In addition, Conti suggests that using small-voxel reconstruction with TOF-PET/CT can improve the detection of small lesions by influencing the image noise levels.[56] The present study revealed that postfiltering with smaller FWHM was more effective in minimizing the negative impact of TOF-PSF-based reconstruction. In PET imaging, the uncertainty in SUVs determination could be caused by several factors, including a matrix size, sphere size (sampling effect), spill out, and aliasing effect. These factors may have a more significant impact on SUVmax since it is more sensitive to noise than SUVmean. It could be concluded that the wider postfiltering values were more effective than the narrower values (mm) in suppressing Gibbs artifact, because the wider postfiltering values successfully reduce the overestimation and underestimation observed in SUVmax for large and small spheres, respectively which is consistent with the observations of other researchers.[33]

In summary, when interpreting PET/CT imaging results, it is essential to be aware of the side effects of PSF algorithm and PVE artifacts on the SUVs measurements, particularly when evaluating lesions of small sizes. Employing appropriate techniques can help mitigate these artifacts, improve the accuracy of the SUVs measurements, and lead to more reliable PET imaging results. Moreover, it is crucial to consider these findings when interpreting PET imaging results and take in considerations the impacts of the matrices sizes, the postfiltering values, and the reconstruction methods on the SUVs measurements.

Limitations

There are several limitations to consider when using spheres with known inner diameters for the current study. First, these spheres may not accurately reflect irregularly shaped lesions with unknown sizes and activity concentrations. Second, the presence of the plastic wall in the spheres could potentially affect the accuracy of the SUVs determination.[57] Furthermore, the outcomes presented in the present study were derived from a predetermined number of iterations and subsets, specifically 2 and 18, respectively. However, it is recommended to explore these parameters further in future investigations to enhance the optimization of reconstruction parameters in PET/CT imaging. Finally, it is important to note that using 2-mm pixels instead of 4 mm can result in approximately four-fold increases in reconstruction time and image storage requirements.[58]

Conclusions

There are various factors that can affect the SUVs measurements in PET imaging, including Gibbs artifacts, PVE, matrices sizes, postfiltering values (mm), and reconstruction techniques. These factors can influence SUVmax and SUVmean quantifications, as well as image noise and spatial resolution, which can have implications for accurate and reliable PET imaging results. To reduce the variability of the SUVs measurements, it is necessary to use sufficient matrix sizes to satisfy sampling criterion and appropriate postfiltering value (mm). Compared to matrix size 192 × 192; a 256 × 256 matrix size with adequate filtration should therefore be used during reconstruction.

The data of the present study are only applicable to our Discovery 710 PET/CT system thus, it is crucial to optimize the PET/CT reconstruction parameters in each hospital according to EANM/EARL recommendations for better SUVs quantification.

Authors' contributions

All authors read and approved the final manuscript.

Availability of data and materials

The datasets used and analyzed during the present study are available upon request.

Financial support and sponsorship

Nil.

Conflicts of interest

There are no conflicts of interest.

References

1. De Luca GM, Habraken JB. Method to determine the statistical technical variability of SUV metrics. EJNMMI Phys 2022;9:40.
2. Itagaki K, Mitsumoto K, Kajisako M, Shioji M, Kawase S. Effect of tumor-pixel positioning on the variability of SUV measurements in PET images. Asia Ocean J Nucl Med Biol 2023;11:71-81.
3. Adams MC, Turkington TG, Wilson JM, Wong TZ. A systematic review of the factors affecting accuracy of SUV measurements. AJR Am J Roentgenol 2010;195:310-20.
4. Boellaard R, O'Doherty MJ, Weber WA, Mottaghy FM, Lonsdale MN, Stroobants SG, *et al.* FDG PET and PET/CT: EANM procedure guidelines for tumour PET imaging: Version 1.0. Eur J Nucl Med Mol Imaging 2010;37:181-200.
5. Kertész H, Conti M, Panin V, Cabello J, Bharkhada D, Beyer T, *et al.* Positron range in combination with point-spread-function correction: An evaluation of different implementations for [124I]-PET imaging. EJNMMI Phys 2022;9:56.
6. Stute S, Comtat C. Practical considerations for image-based PSF and blobs reconstruction in PET. Phys Med Biol 2013;58:3849-70.
7. Marquis H, Willowson KP, Bailey DL. Partial volume effect in SPECT and PET imaging and impact on radionuclide dosimetry estimates. Asia Ocean J Nucl Med Biol 2023;11:44-54.
8. Liu Z, Mhlanga JC, Laforest R, Derenoncourt PR, Siegel BA, Jha AK. A Bayesian approach to tissue-fraction estimation for oncological PET segmentation. Phys Med Biol 2021;66:1-32.
9. Leube J, Claeys W, Gustafsson J, Salas-Ramirez M, Lassmann M, Koole M, *et al.* Position dependence of recovery coefficients in (177)Lu-SPECT/CT reconstructions – Phantom simulations and measurements. EJNMMI Phys 2024;11:52.
10. Bettinardi V, Castiglioni I, De Bernardi E, Gilardi MC. PET quantification: Strategies for partial volume correction. Clin Transl Imaging 2014;2:199-218.
11. Meechai T, Tepmongkol S, Pluempitiwiriyawej C. Partial-volume effect correction in positron emission tomography brain scan image using super-resolution image reconstruction. Br J Radiol 2015;88:1-9.
12. Kinahan PE, Fletcher JW. Positron emission tomography-computed tomography standardized uptake values in clinical practice and assessing response to therapy. Semin Ultrasound CT MR 2010;31:496-505.
13. Zhao J, Jose M. Optimization of Spatial Resolution and Image Reconstruction Parameters for the Small-Animal MetisTM PET/CT System. Electronics [Internet]. 2022;11:1-16. Available from: https://doi.org/10.21203/rs.3.rs-1228467/v1.
14. Aide N, Lasnon C, Desmonts C, Armstrong IS, Walker MD, McGowan DR. Advances in PET/CT Technology: An Update. Seminars in Nuclear Medicine. W.B. Saunders, USA; 2022;52:286-301.
15. Soret M, Bacharach SL, Buvat I. Partial-volume effect in PET tumor imaging. J Nucl Med 2007;48:932-45.
16. Munk OL, Tolbod LP, Hansen SB, Bogsrud TV. Point-spread function reconstructed PET images of sub-centimeter lesions are not quantitative. EJNMMI Phys 2017;4:5.
17. Srinivas SM, Dhurairaj T, Basu S, Bural G, Surti S, Alavi A. A recovery coefficient method for partial volume correction of PET images. Ann Nucl Med 2009;23:341-8.
18. Ashrafinia S, Mohy-Ud-Din H, Karakatsanis NA, Jha AK, Casey ME, Kadrmas DJ, *et al.* Generalized PSF modeling for optimized quantitation in PET imaging. Phys Med Biol 2017;62:5149-79.
19. Watson CC. Estimating effective model kernel widths for PSF reconstruction in PET. IEEE Nucl Sci Symp Conf Rec Val Spain 2011. p. 2368-74.
20. Zeng GL. Gibbs artifact reduction by nonnegativity constraint. J Nucl Med Technol 2011;39:213-9.
21. Rogasch JM, Boellaard R, Pike L, Borchmann P, Johnson P, Wolf J, *et al.* Moving the goalposts while scoring-the dilemma posed by new PET technologies. Eur J Nucl Med Mol Imaging 2021;48:2696-710.
22. van der Vos CS, Koopman D, Rijnsdorp S, Arends AJ, Boellaard R, van Dalen JA, *et al.* Quantification, improvement, and harmonization of small lesion detection with state-of-the-art PET. Eur J Nucl Med Mol Imaging 2017;44:4-16.
23. Bettinardi V, Presotto L, Rapisarda E, Picchio M, Gianolli L, Gilardi MC. Physical performance of the new hybrid PET ∕ CT Discovery-690. Med Phys 2011;38:5394-411.
24. Moretti TJ, Leon SM, Schaeffer CJ, Arreola M. Characterization of time of flight and resolution modeling on image quality in positron emission tomography. J Appl Clin Med Phys 2022;23:e13751.
25. National Electrical Manufacturers Association. Performance Measurements of Positron Emission Tomographs. NEMA Standards Publication NU 2-2007. Rosslyn, VA. 2007.
26. Vennart NJ, Bird N, Buscombe J, Cheow HK, Nowosinska E, Heard S. Optimization of PET/CT image quality using the GE 'Sharp IR' point-spread function reconstruction algorithm. Nucl Med Commun 2017;38:471-9.
27. GE Healthcare, Waukesha, WI, USA. DiscoveryTM PET/CT Series 560, 610 and 710. Learning and Reference Guide.Rev-2, 2015. p. 1–548. Available from: https://www.gehealthcare.com/support/manuals.
28. Knäusl B, Hirtl A, Dobrozemsky G, Bergmann H, Kletter K, Dudczak R, *et al.* PET based volume segmentation with emphasis on the iterative TrueX algorithm. Z Med Phys 2012;22:29-39.
29. EANM/EARL. Accreditation Specifications – EANM EARL – Research4Life; 2018. Available from: https://earl.eanm.org/accreditation-specifications/. [Last accessed on 2023 Feb 14].
30. Kaalep A, Sera T, Rijnsdorp S, Yaqub M, Talsma A, Lodge MA, *et al.* Feasibility of state of the art PET/CT systems performance harmonisation. Eur J Nucl Med Mol Imaging 2018;45:1344-61.
31. Yoon HJ, Jeong YJ, Son HJ, Kang DY, Hyun KY, Lee MK. Optimization of the spatial resolution for the GE discovery PET/CT 710 by using NEMA NU 2-2007 standards. J Korean Phys Soc 2015;66:287-94.
32. Kaalep A, Huisman M, Sera T, Vugts D, Boellaard R. Feasibility of PET/CT system performance harmonisation for quantitative multicentre 89Zr studies. EJNMMI Phys 2018;5.
33. Politte DG, Snyder DL. The use of constraints to eliminate artifacts in maximum-likelihood image estimation for emission tomography. IEEE Trans Nucl Sci 1988;35:608-10.
34. Holman BF, Cuplov V, Millner L, Hutton BF, Maher TM, Groves AM, *et al.* Improved correction for the tissue fraction effect in lung PET/CT imaging. Phys Med Biol 2015;60:7387-402.
35. Adler S, Seidel J, Choyke P, Knopp MV, Binzel K, Zhang J, *et al.* Minimum lesion detectability as a measure of PET system performance. EJNMMI Phys 2017;4:13.
36. Snyder DL, Miller MI, Thomas LJ, Politte DG. Noise and edge artifacts in maximum-likelihood reconstructions for emission tomography. IEEE Trans Med Imaging 1987;6:228-38.

37. Tsutsui Y, Awamoto S, Himuro K, Umezu Y, Baba S, Sasaki M. Edge artifacts in point spread function-based PET reconstruction in relation to object size and reconstruction parameters. Asia Ocean J Nucl Med Biol 2017;5:134-43.
38. Rogasch JM, Steffen IG, Hofheinz F, Großer OS, Furth C, Mohnike K, *et al.* The association of tumor-to-background ratios and SUVmax deviations related to point spread function and time-of-flight F18-FDG-PET/CT reconstruction in colorectal liver metastases. EJNMMI Res 2015;5:31.
39. Ahn S. Theoretical analysis of resolution and noise properties of PET image reconstruction with and without sinogram blurring modeling. IEEE Nucl Sci Symp Med Imaging Conf NSS/MIC 2014;6:1-4.
40. Boellaard R, Delgado-Bolton R, Oyen WJ, Giammarile F, Tatsch K, Eschner W, *et al.* FDG PET/CT: EANM procedure guidelines for tumour imaging: Version 2.0. Eur J Nucl Med Mol Imaging 2015;42:328-54.
41. Gavriilidis P, Koole M, Marinus A, Jansen FP, Deller TW, Mottaghy FM, et al. Performance evaluation of iterative PET reconstruction with resolution recovery incorporating Gallium-68 positron range correction. Med Phys 2024;51:1-16.
42. Tong S, Alessio AM, Kinahan PE. Noise and signal properties in PSF-based fully 3D PET image reconstruction: An experimental evaluation. Phys Med Biol 2010;55:1453-73.
43. Rep S, Tomše P. PET/CT NEMA Body Phantom Image Reconstruction Study Using 2 mm Voxel Size for Improved Image Quality. Vol. PREPRINT, Research Square. 2021. doi: 10.21203/rs.3.rs-204140/v1.
44. Chauvie S, Bergesio F, De Ponti E, Morzenti S, De Maggi A, Ragazzoni M, *et al.* The impact of time-of-flight, resolution recovery, and noise modelling in reconstruction algorithms in non-solid-state detectors PET/CT scanners: Multi-centric comparison of activity recovery in a 68Ge phantom. Phys Med 2020;75:85-91.
45. Aide N, Lasnon C, Kesner A, Levin CS, Buvat I, Iagaru A, *et al*. New PET technologies – Embracing progress and pushing the limits. Eur J Nucl Med Mol Imaging 2021;48:2711-26.
46. Zimmermann PA, Houdu B, Césaire L, Nakouri I, De Pontville M, Lasnon C, *et al.* Revisiting detection of in-transit metastases in melanoma patients using digital (18)F-FDG PET/CT with small-voxel reconstruction. Ann Nucl Med 2021;35:669-79.
47. Riegler G, Karanikas G, Rausch I, Hirtl A, El-Rabadi K, Marik W, *et al.* Influence of PET reconstruction technique and matrix size on qualitative and quantitative assessment of lung lesions on [18F]-FDG-PET: A prospective study in 37 cancer patients. Eur J Radiol 2017;90:20-6.
48. Capotosti A, Moretti R, Milano A, Nardini M, Cusumano D, Annunziata S, *et al*. Up-to-Date Optimization of the 90Y-PET/CT Reconstruction Protocol for Volumetric Quantification in Trans-Arterial RadioEmbolization (TARE) Procedures in the Era of Theranostics. Appl Sci 2022;12:1-9.
49. Ptáček J, Karhan P, Fiala P. Optimal reconstruction matrix and PET image filtration for point-spread function and time-of-flight reconstruction – A phantom study. Phys Med 2017;39:95-9.
50. INTERNATIONAL ATOMIC ENERGY AGENCY. PET/CT Atlas on Quality Control and Image Artefacts. IAEA Human Health Series No. 27, Vienna. 2014 [cited 2024 Jun 5]. 1–108 p. Available from: http://www.iaea.org/Publications/index.html.
51. Brendle C, Kupferschläger J, Nikolaou K, la Fougère C, Gatidis S, Pfannenberg C. Is the standard uptake value (SUV) appropriate for quantification in clinical PET imaging? Variability induced by different SUV measurements and varying reconstruction methods. Eur J Radiol 2015;84:158-62.
52. Hashimoto N, Morita K, Tsutsui Y, Himuro K, Baba S, Sasaki M. Time-of-flight information improved the detectability of subcentimeter spheres using a clinical PET/CT scanner. J Nucl Med Technol 2018;46:268-73.
53. Roef MJ, van den Berg K, Rutten HJ, Burger J, Nederend J. The additional role of F18-FDG PET/CT in characterizing MRI-diagnosed tumor deposits in locally advanced rectal cancer. Tomography 2024;10:632-42.
54. Dickson JC, Armstrong IS, Gabiña PM, Denis-Bacelar AM, Krizsan AK, Gear JM, *et al.* EANM practice guideline for quantitative SPECT-CT. Eur J Nucl Med Mol Imaging 2023;50:980-95.
55. Lois C, Jakoby BW, Long MJ, Hubner KF, Barker DW, Casey ME, *et al.* An assessment of the impact of incorporating time-of-flight information into clinical PET/CT imaging. J Nucl Med 2010;51:237-45.
56. Koopman D, van Dalen JA, Lagerweij MC, Arkies H, de Boer J, Oostdijk AH, *et al.* Improving the detection of small lesions using a state-of-the-art time-of-flight PET/CT system and small-voxel reconstructions. J Nucl Med Technol 2015;43:21-7.
57. Berthon B, Marshall C, Edwards A, Evans M, Spezi E. Influence of cold walls on PET image quantification and volume segmentation: A phantom study. Med Phys 2013;40:(082505-1)-(082505-13).
58. Morey AM, Noo F, Kadrmas DJ. Effect of using 2mm voxels on observer performance for PET lesion detection. IEEE Trans Nucl Sci 2016;63:1359-66.